PCCP

PAPER

View Article Online
View Journal | View Issue

Cite this: *Phys. Chem. Chem. Phys.*, 2017, **19**, 25537

Acid- and hydrogen-bonding-induced switching between 22-π and 18-π electron conjugations in 2-aminothiazolo[4,5-*c*]porphycenes†

Oriol Planas,[a] Daniel Fernández-Llaneza,[a] Ingrid Nieves,[a] Rubén Ruiz-Gonzalez,[a] Else Lemp,[b] Antonio L. Zanocco[b] and Santi Nonell*[a]

Received 4th May 2017,
Accepted 27th August 2017

DOI: 10.1039/c7cp02938a

rsc.li/pccp

2-Aminothiazolo[4,5-*c*]porphycenes are a novel class of 22-π electron aromatic porphycene derivatives prepared by click reaction of porphycene isothiocyanates with primary and secondary amines with high potential as near-infrared theranostic labels. Herein, the optical and photophysical properties of 2-aminothiazolo[4,5-*c*]porphycenes have been studied, revealing a strong dependence on hydrogen bond donor solvents and acids. High hydrogen bond donor solvents and acids shift the absorption and fluorescence emission of 2-aminothiazolo[4,5-*c*]porphycenes to the blue due to a contraction of their aromatic system from 22-π to 18-π electrons. Finally, the aromatic shift has been successfully used to measure the pH using 2-aminothiazoloporphycene-labelled gold nanoclusters, paving the way for the use of these compounds as near infrared pH-sensitive probes.

Introduction

Porphycenes are [4*n* + 2]-π electron aromatic porphyrinoids consisting of two bipyrroles linked by ethylene bridges. These macrocycles were first synthesised by Vogel *et al.* in 1986, who named them porphycenes since their structure combines features of both porphyrins and acenes.[1] Their isolation and structural characterisation open up new avenues for the research in multiple fields such as photodynamic therapy,[2–5] organic solar cells,[6–8] catalysis[9,10] and theranostics.[11] Over the last decade, the photophysical properties of symmetric and asymmetric 18-π porphycene derivatives have been studied, revealing specific properties such as the *N-H* tautomerization[12,13] or nonlinear optical properties[14–16] which set them apart from other related 18-π porphyrinoids. Of particular interest is the *N-H* tautomerization process in 9-substituted asymmetric porphycene derivatives as high electron-donating substituents in the 9-position leads to an enhanced energetic–splitting between the two *trans*-tautomers resulting in dual fluorescence emission.[17–19] In contrast, little is known about the properties of higher conjugated ($n > 4$) aromatic porphycenes.

Two main families of expanded [4*n* + 2]-π ($n > 4$) porphycene macrocycles can be distinguished as expanded and fused-porphycenes. The expanded porphycenes result from the insertion of sp- or sp^2-hybridized carbons or heterocyclic rings into the bridge connecting the pyrroles.[20,21] On the other side, fused-porphycenes result from the fusion of cycles containing sp- or sp^2- carbons or heteroatoms in the β,β′[22] or *meso*-positions[11,23,24] of the macrocycle. Both porphycene families have red-shifted absorption and fluorescence spectra with respect to their parent 18-π as a result of the larger aromatic system.[11,23–25] Of specific interest are *meso*-fused porphycene derivatives since this position is highly sensitive to the substituent nature.[18] However, their study has been challenging owing to difficult synthetic preparation[26] and extremely low emission quantum yields.[27]

We recently reported the spontaneous formation of 2-aminothiazolo[4,5-*c*]porphycenes upon click reaction of 9-isothiocyanate porphycene derivatives (PoITCs) with primary and secondary amines (Fig. 1). Interestingly, the fused 2-aminothiazolo[4,5-*c*]porphycenes are endowed with red-shifted absorption and fluorescence emission spectra compared with their precursors, which were explained on the grounds of an expanded 22-π electronic delocalization. Moreover PoITCs could satisfactorily label amino-containing biomolecules and gold nanoclusters yielding thiazoloporphycene conjugates with near-infrared fluorescence emission and also capable of photosensitising the production of the cytotoxic species singlet oxygen. Thus, 2-aminothiazolo[4,5-*c*]-porphycenes are aromatic 22-π electron porphycenes of particular interest for phototheranostic applications.

In the course of our studies on the photophysical properties of 2-aminothiazolo[4,5-*c*]porphycenes and their conjugates, we observed dual fluorescence emission from some of the bio- and nanoconjugates, which prompted us to investigate its origin

[a] *Institut Químic de Sarrià, Universitat Ramon Llull, Via Augusta 390, Barcelona 08017, Spain. E-mail: santi.nonell@iqs.url.edu*
[b] *Facultad de Ciencias Químicas y Farmacéuticas, Universidad de Chile, Sergio Livingstone 1007, Santiago, Chile*

† Electronic supplementary information (ESI) available. See DOI: 10.1039/c7cp02938a

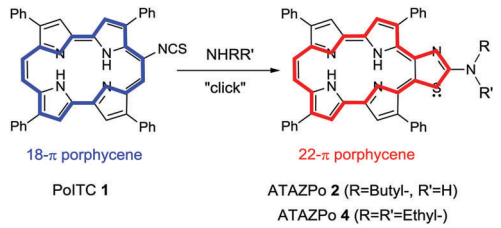

Fig. 1 Reaction of porphycene isothiocyanates with primary or secondary amines (NHRR') to yield 22-π electron aromatic 2-aminothiazolo[4,5-*c*]-porphycenes.

further. Previously, we had observed dual emission in 9-substituted porphycenes and this was rationalised as resulting from inner-*NH* tautomerization.[17,18] Herein we describe the solvent effects on the optical and photophysical properties of 2-aminothiazolo[4,5-*c*]-porphycenes. According to our results, the aromaticity of 2-aminothiazolo[4,5-*c*]porphycenes can be reversibly switched between 22-π and 18-π electron systems by H-bond donating solvents and acids. We further show that this effect can be exploited for the design of novel fluorescent pH sensors in the near-infrared.

Experimental

Chemicals

9-Isothiocyanate-2,7,12,17-tetraphenylporphycene (PoITC **1**), 2-(*N*-butylamino)thiazolo[4,5-*c*]2,7,12,17-tetraphenyl-porphycene (ATAZPo **2**), 2-phenylthiazolo[4,5-*c*]2,7,12,17-tetraphenylporphycene (TAZPo **3**) and 2-(*N*,*N*-diethylamino) thiazolo[4,5-*c*]2,7,12,17-tetraphenylporphycene (ATAZPo **4**) were synthesized as previously described by Planas *et al.*[11] and found to be of purity >95% by HPLC (see ESI†). All solvents used were of spectroscopic grade quality unless otherwise stated. Formic, acetic, propionic, lactic, hydrochloric, sulfuric, nitric, phosphoric, and boric acids were of analytical grade quality and were used as received.

Synthesis of tetraethyleneglycol undecyl-thiol stabilised gold nanoclusters

30 mg of 23-mercapto-3,6,9,12-tetraoxatricosan-1-ol (90 μmol) and 3.3 mg of 1-amino-3,6,9,12-tetraoxatricosane-23-thiol (10 μmol) were mixed with 10 mg of tetrachloroauric acid trihydrate (30 μmol) in 7.0 mL of methanol. 0.6 mL of a freshly prepared solution of $NaBH_4$ (1.3 M) was added slowly. The mixture was stirred at room temperature during 2.5 h and then the solvent was removed under reduced pressure. Next, the remaining crude was dispersed in water and purified by dialysis twice (24 h, 800 mL). The aqueous solution was basified using a 0.1 M solution of KOH and extracted several times with $CHCl_3$. The organic layers were dried over anhydrous Na_2SO_4 and the solvent was removed under reduced pressure. Finally, the brownish solid powder was suspended in 20 mL of absolute ethanol. This process has been adapted from ref. 28.

Labelling of tetraethylenglycol undecyl-thiol stabilized gold nanoclusters with PoITC 1

20 mg of amino-containing gold nanoclusters were dissolved in 5 mL of absolute ethanol and then mixed with 150 μL of 9-isothiocyanate-2,7,12,17-tetraphenylporhycene (2 mM) in dichloromethane. Catalytic amounts of anhydrous potassium carbonate were added in order to favour the amine deprotonation and subsequent nucleophilic addition. The mixture was stirred at room temperature for 72 h. After the reaction completion, the solvent was removed under reduced pressure and the powder redispersed in absolute ethanol. The reaction crude was purified using a Sephadex LH20 column using ethanol as mobile phase.

General spectroscopic techniques

All spectroscopic measurements were carried out in 1 cm quartz cuvettes (Hellma, Germany) in air-saturated solutions at room temperature using spectroscopic grade solvents. Absorption spectra were recorded using a double beam UV-Vis-NIR Varian Cary 6000i spectrophotometer. Fluorescence emission and excitation spectra were registered using a Jobin-Yvon-Spex FLUOROMAX-4 spectrofluorometer using a long-pass filter cutting at 550 nm (Thorlabs) when required. Time-resolved fluorescence decays were measured using a PicoQuant Fluotime 200 time-correlated fluorescence lifetime spectrophotometer, with excitation at 375 nm.

Linear solvation energy relationships

ATAZPo **2** was dissolved in nineteen solvents of different polarity, H-bond donor (HBD) and H-bond acceptor (HBA) properties at a final concentration of 1.3 μM and its absorption spectra were subsequently collected. The dependence of the absorption maximum position on microscopic solvent parameters was analysed in terms of linear solvation energy relationships (LSER) employing the semiempirical solvatochromic equations of Taft, Kamlet *et al.* (eqn (1))[29,30] and Catalán (eqn (2)).[31,32]

$$\bar{\nu}_A = \bar{\nu}_0 + a\pi^* + d\delta + b\alpha + c\beta \quad (1)$$

$$\bar{\nu}_A = \bar{\nu}_0 + a\mathrm{SPP} + b\mathrm{SA} + c\mathrm{SB} \quad (2)$$

where $\bar{\nu}_A$ corresponds to the wavenumber of the absorption maximum, π* accounts for the polarizability and dipolarity of the solvent, δ is a correction term for polarizability, α corresponds to the HBD solvent ability and β indicates solvent capability as a HBA.[33–35] Similarly, SPP in eqn (2) is related to the solvent ability to stabilize charges or dipoles, SA to its HBD capacity and SB to its HBA capability.[31,32] The coefficients of the LSER equations were obtained by multilinear regression analysis using the statistical software Statview. Sample size, *N*, the product correlation coefficient, *R*, and the Fisher index of equation reliability, *F*, were taken as indicators of the goodness of the fit. Suitable fittings are indicated by large *N* and *R* values and *F* close to one.

Determination of acid–base equilibrium constants

The acid–base equilibrium constant (*K*) between ATAZPo **2** and an acid (HA), was defined by eqn (3):

$$K = \frac{[\mathrm{ATAZPo} - \mathrm{H}^+][\mathrm{A}^-]}{[\mathrm{ATAZPo}][\mathrm{HA}]} \quad (3)$$

ATAZPo **2** was dissolved in MeOH at a final concentration of 1.3 μM and its absorption and fluorescence spectra were

collected after adding increasing volumes of an acid stock solution. The concentration-dependent evolution of the absorption spectra was globally analysed using the Specfit/32 software (Spectrum Software Associates) to yield K. However, Specfit did not render acceptable fitting results when changes in the absorption spectra were very small. In such cases, fluorescence emission data from all samples were analysed using Benesi–Hildebrand's method (eqn (4)):[36]

$$\frac{1}{I - I_0} = \frac{1}{I_\infty - I_0}\left(1 + \frac{1}{K} \times \frac{1}{[\mathrm{HA}]}\right) \quad (4)$$

where I is the fluorescence intensity at a given concentration of the acid ([HA]), I_0 is the fluorescence intensity when no acid has been added and I_∞ is the fluorescence intensity when all porphycene molecules are effectively complexed. Plots of $1/(I - I_0)$ *vs.* 1/[HA] yielded the K values.

Fluorescence emission of porphycene-labelled conjugates

Fluorescence emission of porphycene-labelled tetraethylene-glycol undecyl-thiol stabilized gold nanoclusters at different pH was measured by dissolving the conjugate in citric acid/Na_2HPO_4 buffer of different concentrations. Table S1 (ESI†) shows the proportions of solutions of citric acid 0.1 M and Na_2HPO_4 0.2 M to prepare 100 mL of buffer at different pH values.

Results and discussion

Solvent effects on the absorption and emission of ATAZPo 2

As a first step, the absorption spectrum of ATAZPo **2** was measured in a range of solvents of different polarity, H-bond donor (HBD) and H-bond acceptor (HBA) capacity to identify the molecular properties with the highest contribution to solvents effects (Fig. 2). The shape of the spectra is almost identical for all solvents except for high HBD fluorinated alcohols 2,2,2-trifluoroethanol (TFE) and, particularly, 1,1,1,3,3,3-hexafluoro-2-propanol (HFIP). In non-HBD solvents the lowest-energy band shifts slightly to longer wavelengths upon increasing the solvent polarity and their HBA capacity. In mixtures of HFIP and MeOH a gradual conversion of the near-IR-absorbing species to the red-absorbing species is observed concomitant to increasing the percentage of HFIP (Fig. S5 in the ESI†). Clearly, the electronic π system of ATAZPo **2** is severely perturbed by HBD solvents.

An analogous trend can be observed in the fluorescence emission spectra (Fig. 2, λ_{exc} = 598 nm) and lifetime (Fig. S5 in the ESI†). In non-HBD solvents ATAZPo **2** shows a single near-infrared emission band (F_1) at around λ = 760 nm, which shows similar solvent shifts as the absorption spectra. In HBD solvents, a second emission band (F_2) appears at approximately λ = 680 nm. This band is dominant in HFIP while both F_1 and F_2 emission bands can be observed in TFE. The excitation spectra recorded observing at the edges of the F_1 and F_2 emission bands both in HFIP and MeOH match the respective absorption spectra in these solvents (Fig. S6, ESI†). In contrast, the excitation spectrum in TFE depends on the observation wavelength (Fig. S6, ESI†), which indicates that more than one fluorescent species is present in TFE solutions. Regarding lifetimes, a decrease can be observed from MeOH (0.7 ns) to HFIP (0.4 ns).

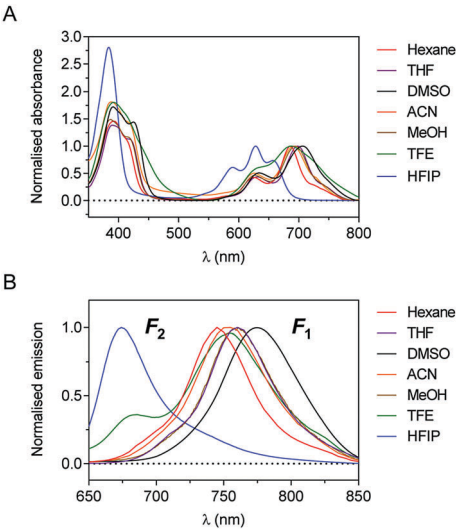

Fig. 2 Absorption (A) and emission spectra (B, λ_{exc} = 598 nm) of ATAZPo **2** in different solvents.

A deeper understanding of the solvent-induced shifts on the absorption spectra was gained from the LSER analysis. Multi-linear fitting using Taft (π*, α and β, eqn (1)) and Catalan (SPP, SA and SB, eqn (2)) solvent parameters of a set of nineteen solvents afforded suitable correlation equations with large values of F and with R values close to 1 (Fig. S7, ESI†). The parameter coefficients collected in Table S2 (ESI†) show that HBA solvents (with large values of β or SB) mainly dominate the solvent effect, causing small shifts of the absorption maxima towards near-IR wavelengths. In addition, the negative value of the coefficients associated with π* and SPP indicate that the absorption maximum is also shifted to lower wavelengths in solvents able to stabilize charges or dipoles. In contrast, the positive value of the coefficient associated with α or SA parameters shows that HBD solvents shifts the absorption maximum towards lower wavelengths, but its small value suggests that only very strong HBD solvents induce significant changes. Results of LSER analysis, *i.e.*, the moderate effect of HBA solvents on the position of the low energy absorption band of ATAZPo **2**, the practically null effect of HBD solvents and the appearance of a new band in the red in very strong HBD solvents, suggest that different forms of ATAZPo **2** are present in HBA or in extremely strong HBD media.

Taken together, the results from absorption and fluorescence measurements clearly indicate that non-HBD solvents stabilize a form of ATAZPo **2** with near-IR absorption and emission bands, while high HBD solvents stabilize a different species that absorbs and emits in the red.

Acid effects on the absorption and emission of ATAZPo 2

The results above indicate that the absorption and fluorescence spectra of ATAZPo **2** are very sensitive to proton donors. Further insight was gained by studying the protonation of ATAZPo **2** with acids of different strength. A total of 9 acids were tested, including 5 mineral acids (HCl, HNO_3, H_2SO_4, H_3BO_3 and H_3PO_4)

and 4 organic acids (formic, acetic, propionic and lactic acid). All acids were able to induce spectral changes similar to those observed in HBD solvents in a concentration and acid-strength dependent manner (see Fig. S7 and S8 in the ESI†). The acid–base equilibrium constant between ATAZPo **2** and each acid was determined from spectral analysis using either the Specfit software or Benesi–Hildebrand plots. There was an excellent agreement between the Specfit and the Benesi–Hildebrand results for those acids that induced large spectral changes (Table 1). However, Specfit failed to yield reliable fits for weaker acids and only the Benesi–Hildebrand results were deemed acceptable.

A plot of log K against pK_a shows a linear relationship spanning 20 pK_a units (Fig. 3).

Time-resolved fluorescence spectroscopy provided further insight on the effects of HFIP and acids on the electronic structure of ATAZPO **2**. Thus, the fluorescence decay lifetimes were 0.7 ns in MeOH, 0.4 ns in HFIP but eight-fold smaller, 0.05 ns, in MeOH/HCl 5 mM, suggesting that species formed in the two solvents are different, despite showing similar spectral features.

Solvent and acid effects on other porphycenes

The results thus far indicate that ATAZPo **2** can interconvert between red- and near-infrared absorbing and emitting species in response to HBD solvents and acids. In most 18-π tetrapyrroles including porphycenes, protonation does not change the extension of conjugation. As a result the position of the bands changes only slightly, the major changes being in their relative intensities owing to modification of the transition probabilities as a result of the symmetry changes.[38] Thus, in order to assess the origin and relevance of our observations, additional tests were conducted. First, the absorption and emission spectra of a related porphycene lacking the aminothiazole moiety (2,7,12,17-tetraphenylporphycene, TPPo) were measured in the presence of HFIP and HCl (Fig. S10 in the ESI†). No spectral changes could be observed in either case, which rules out protonation of the pyrrole nitrogens as the underlying cause for the observed results for ATAZPo **2** and sets this molecule apart of any porphycene reported so far. Prompted by our previous observations that the tautomers of asymmetric 9-amino porphycenes showed distinct red and near-IR absorption and fluorescence spectra,[17,18] we next considered the possibility that the two extreme spectra observed for the also asymmetric ATAZPo **2** could correspond to two tautomers as well, whose relative population would be affected by the solvent properties. The absorption spectra of 9-amino-2,7,12,17-tetrakis(2-methoxy ethyl) porphycene in HFIP and in THF (Fig. S11 in the ESI†) show however that the tautomeric equilibrium is not affected by HFIP suggesting that this possibility can be safely ruled out. Additional insight was gained from the effect of HFIP on the absorption and time resolved fluorescence emission spectra of a thiazoloporphycene (TAZPo **3**) that lacks the amino group attached to the thiazole. For this compound, HFIP was unable to cause the same kind of spectral and fluorescence lifetime changes that we observed for 2-aminothiazoloporphycenes (Fig. S12 in the ESI†), further ruling out the hypothesis that neutral and protonated forms exist in different tautomeric structures.

Finally, since in ATAZPo **2** an amino-imino *N-H* prototropism at the aminothiazole moiety is also possible, this hypothesis was considered as well. However ATAZPo **4**, an aminothiazolo porphycene unable to undergo such prototropism, was nevertheless affected by HFIP and acid in a similar way as ATAZPo **2** (Fig. S13 in the ESI†), ruling out the amino–imino tautomerization hypothesis as well. Fig. 5 summarises the above findings for the different thiazolopophycenes.

Table 1 Logarithm of the equilibrium constant of ATAZPo **2** with mineral and organic acids

Acid	pK_a [a]	log(K) [b]	log(K) [c]
HCl	−8.00	2.41	3.1
H_2SO_4	−3.0	1.82	1.6
HNO_3	−1.3	1.29	1.3
H_3PO_4	2.1	0.25	−0.1
Formic acid	3.3	−0.71	−0.7
Lactic acid	3.9	—	−0.9
Acetic acid	4.8	—	−0.8
Propionic acid	4.9	—	−0.7
H_3BO_3	9.3	—	−1.5

[a] Ref. 37. [b] Determined using SpecFit. [c] Determined using Benesi–Hildebrand plots.

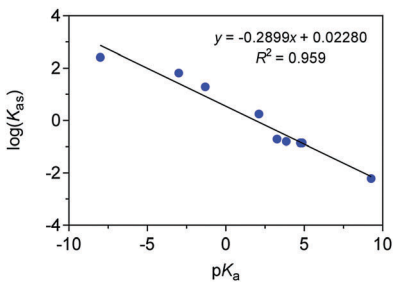

Fig. 3 Linear correlation between the logarithm of the association constant between ATAZPo **2** and acids *versus* their pK_a.

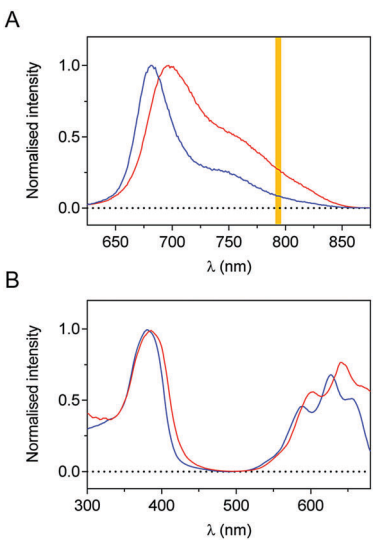

Fig. 4 Emission (A, λ_{exc} = 598 nm) and excitation spectra (B, λ_{obs} = 790 nm) of ATAZPo **2** in MeOH with 50% of HFIP (blue) and in MeOH with 1% HCl (red).

Discussion

The results presented in the previous sections indicate that the lowest-energy bands in the absorption and fluorescence spectra of 2-aminothiazoloporphycenes shift from the near-infrared to the red upon addition of HBD solvents and acids. 2-Aminothiazoloporphycenes are formed by reaction of 9-isothiocyanatoporphycenes with amines which expands the aromatic π system from 18 to 22 electrons, leading to a large red-to-near-IR spectral shift.[11] It is remarkable that the addition of HBD solvents and acids to 2-aminothiazoloporphycenes induces the opposite effect, yielding the typical spectra of 18-π porphycenes.[39] This suggests that the aromatic system in 2-aminothiazoloporphycenes has been reduced from 22-π to 18-π electrons by HBD solvents and acids, which is unprecedented in porphycenes and other porphyrinoids. The similarity of the spectra in HBD solvents and acids (Fig. 4) suggests protonation as the common underlying cause. It seems reasonable to hypothesize that HFIP forms a very strong hydrogen bond with the endocyclic nitrogen of the 2-aminothiazoloporphycene, which would effectively interrupt the 22-π conjugation pathway and stabilise an 18-π aromatic zwitterionic structure (Fig. 6). In the case of acids, a full proton transfer to the endocyclic nitrogen, which is the most basic nitrogen in 2-aminothiazolo compounds,[40–42] would also yield

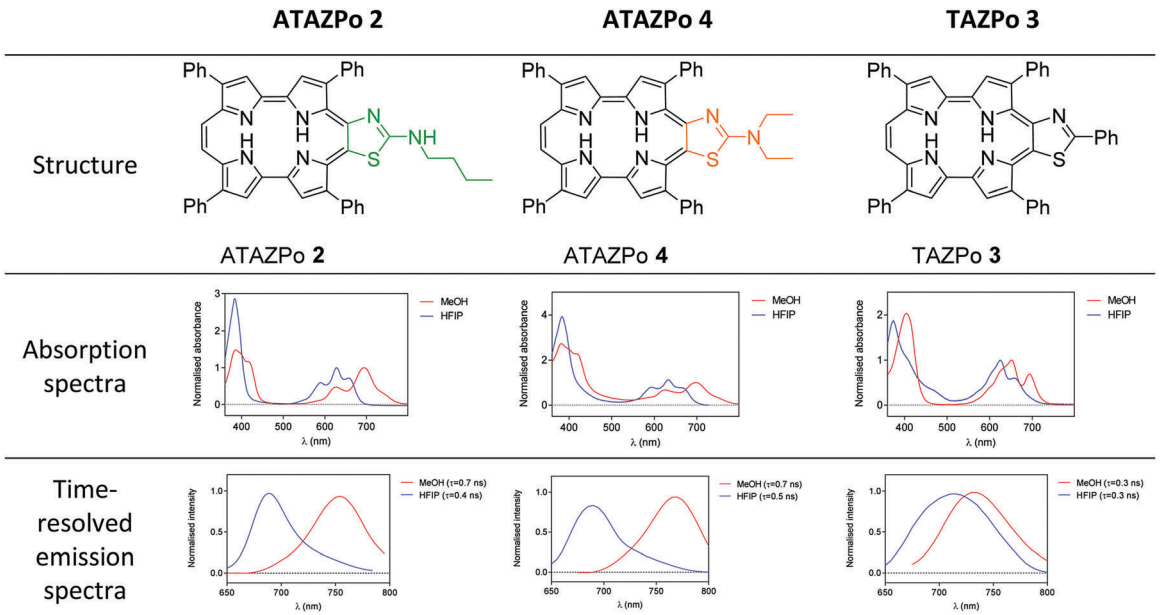

Fig. 5 Comparison of the solvent effects on the absorption and emission spectra of different thiazoloporphycenes.

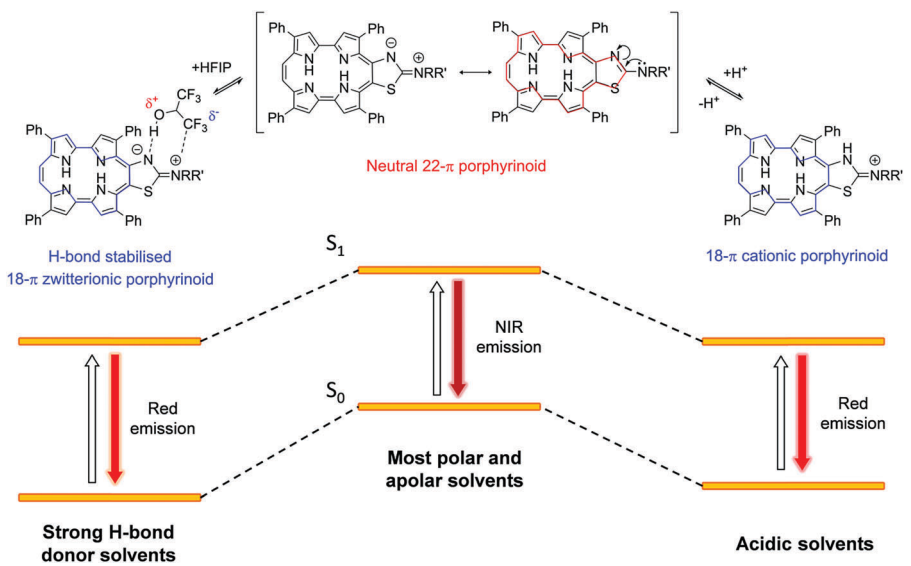

Fig. 6 Proposed structures and energy diagrams of 2-aminothiazolo[4,5-*c*]porphycenes in different media.

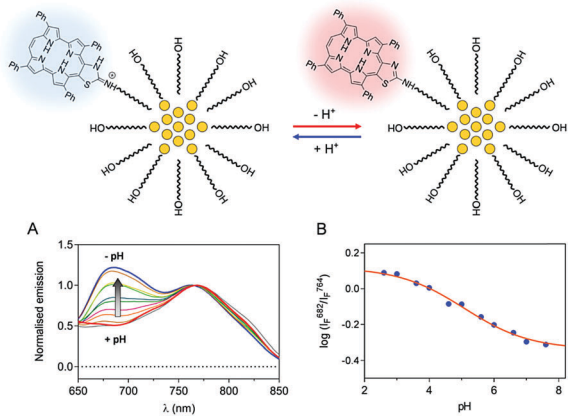

Fig. 7 pH detection by 2-aminothiazolo[4,5-*c*]porphycene-labelled gold nanoclusters. (A) pH dependent fluorescence emission spectra of AuNCs-porphycene conjugates (λ_{exc} = 580 nm) and (B) plot of the ratio of emission maxima of the blue- and red-shifted spectra (centred at 682 nm and 764 nm, respectively) *versus* the pH.

an 18-π aromatic structure, although cationic in this case. As both structures are isoelectronic, the spectra are expected to be very similar, in agreement with the experimental observations.

An alternative explanation could also be considered whereby the one that is responsible for the conversion of the 22-π to the 18-π aromatic system would not be the lone pair migration from the exocyclic *NRR'* but from the *S* of the thiazole ring. In this scenario, HFIP would also form a hydrogen bond with the negatively charged endocyclic *N* but its negatively charged CF_3 moiety would interact instead with the positively charged sulphur atom. However, the observation that HFIP does not convert the 22-π aromatic conjugation of TAZPo **3** to the corresponding 18-π aromatic system rules out such possibility.

Application: labelling of nanostructures for pH measurements

The spectral changes observed in HBD solvents and in the presence of acids suggest that 2-aminothiazolo[4,5-*c*]porphycenes have a strong potential as red/near-IR acidity/H-bonding probes. However, thiazoloporphycenes are hydrophobic, therefore we labelled them onto gold nanoclusters for solubilisation in aqueous media and exposed them to citrate/phosphate buffers of different pH.

As expected, dual red and near-IR fluorescence was detected from all samples, whereas the intensity ratio of the two bands changed in a pH-dependent manner (Fig. 7). Thus, thiazoloporphycenes were effective ratiometric pH indicators in the working range from pH 2.6 to 7.6, with a pK_a value close to 5.0, which might be ideal for probing the acidity of biological compartments. Work is currently in progress to explore this application in detail.

Conclusions

The optical properties of 2-aminothiazolo[4,5-*c*]porphycenes are highly dependent on the HBD and acidity properties of the solvent. In such environments, the absorption and fluorescence emission of 2-aminothiazolo[4,5-*c*]porphycenes shift to the blue due to the stabilisation of a smaller aromatic system. Hence, the 22-π aromatic system of 2-aminothiazolo[4,5-*c*]porphycenes that confers them with near-IR absorption and emission properties in polar and non-polar solvents, is substituted by 18-π electron aromatic systems in high HBD solvents and in the presence of acids. This switching has been successfully used to measure the pH of aqueous media using gold nanoclusters labelled with 2-aminothiazolo-porphycene, paving the way for the use of these novel expanded porphycenes as red/near-IR probes of proticity and H-bonding ability of microenvironments.

Conflicts of interest

There are no conflicts of interest to declare.

Acknowledgements

Financial support for this research was obtained from the Spanish Ministerio de Economía y Competitividad (Grants No. CTQ2013-48767-C3-1-R, CTQ2016-78454-C2-1-R and CTQ2015-71896-REDT). O. P. thanks the European Social Funds and the SUR del DEC de la Generalitat de Catalunya for his predoctoral fellowship (Grant No. 2016 FI_B2_00100).

References

1 E. Vogel, M. Köcher, H. Schmickler and J. Lex, *Angew. Chemie Int. Ed.*, 1986, **25**, 257–259.
2 J. C. Stockert, M. Cañete, A. Juarranz, A. Villanueva, R. W. Horobin, J. I. Borrell, J. Teixido and S. Nonell, *Curr. Med. Chem.*, 2007, **14**, 997–1026.
3 X. Ragàs, D. Sánchez-García, R. Ruiz-González, T. Dai, M. Agut, M. R. Hamblin and S. Nonell, *J. Med. Chem.*, 2010, **53**, 7796–7803.
4 M. García-Díaz, D. Sánchez-García, J. Soriano, M. L. Sagristà, M. Mora, Á. Villanueva, J. C. Stockert, M. Cañete and S. Nonell, *MedChemComm*, 2011, **2**, 616–619.
5 R. Ruiz-González, P. Acedo, D. Sánchez-García, S. Nonell, M. Cañete, J. C. Stockert and A. Villanueva, *Eur. J. Med. Chem.*, 2013, **63**, 401–414.
6 R. D. Costa, J. Malig, W. Brenner, N. Jux and D. M. Guldi, *Adv. Mater.*, 2013, **25**, 2600–2605.
7 W. Brenner, J. Malig, R. D. Costa, D. M. Guldi and N. Jux, *Adv. Mater.*, 2013, **25**, 2314–2318.
8 S. Feihl, R. D. Costa, W. Brenner, J. T. Margraf, R. Casillas, O. Langmar, A. Browa, T. E. Shubina, T. Clark, N. Jux and D. M. Guldi, *Chem. Commun.*, 2014, **50**, 11339–11342.
9 D. Maeda, H. Shimakoshi, M. Abe and Y. Hisaeda, *Dalton Trans.*, 2009, 140–145.
10 K. Oohora, Y. Kihira, E. Mizohata, T. Inoue and T. Hayashi, *J. Am. Chem. Soc.*, 2013, **135**, 17282–17285.
11 O. Planas, T. Gallavardin and S. Nonell, *Chem. Commun.*, 2015, **51**, 5586–5589.

12 T. Kumagai, F. Hanke, S. Gawinkowski, J. Sharp, K. Kotsis, J. Waluk, M. Persson and L. Grill, *Nat. Chem.*, 2014, **6**, 41–46.
13 J. Waluk, *Chem. Rev.*, 2017, **117**, 2447–2480.
14 T. Sarma, P. K. Panda, P. T. Anusha and S. V. Rao, *Org. Lett.*, 2011, **13**, 188–191.
15 S. Venugopal Rao, T. Shuvan Prashant, D. Swain, T. Sarma, P. K. Panda and S. P. Tewari, *Chem. Phys. Lett.*, 2011, **514**, 98–103.
16 A. Rana, S. Lee, D. Kim and P. K. Panda, *Chem. Commun.*, 2015, **51**, 7705–7708.
17 M. Duran-Frigola, R. Tejedor-Estrada, D. Sánchez-García and S. Nonell, *Phys. Chem. Chem. Phys.*, 2011, **13**, 10326–10332.
18 O. Planas, R. Tejedor-Estrada and S. Nonell, *J. Porphyrins Phthalocyanines*, 2012, **16**, 633–640.
19 O. Planas, T. Gallavardin and S. Nonell, in *Handbook of Porphyrin Science*, ed. R. Guilard, K. M. Smith and K. M. Kadish, World Scientific Publishers, 2016, vol. 41, pp. 299–349.
20 N. Jux, P. Koch, H. Schmickler, J. Lex and E. Vogel, *Angew. Chem., Int. Ed.*, 1990, **29**, 1385–1387.
21 E. Vogel, N. Jux, E. Rodriguez-Val, J. Lex and H. Schmickler, *Angew. Chem., Int. Ed.*, 1990, **29**, 1387–1390.
22 D. Kuzuhara, J. Mack, H. Yamada, T. Okujima, N. Ono and N. Kobayashi, *Chemistry*, 2009, **15**, 10060–10069.
23 K. Oohora, A. Ogawa, T. Fukuda, A. Onoda, J. Hasegawa and T. Hayashi, *Angew. Chem., Int. Ed.*, 2015, **54**, 6227–6230.
24 D. Kuzuhara, M. Sakaguchi, W. Furukawa, T. Okabe, N. Aratani and H. Yamada, *Molecules*, 2017, **22**, 1–15.
25 D. Kuzuhara, H. Yamada, S. Mori, T. Okujima and H. Uno, *J. Porphyrins Phthalocyanines*, 2011, **15**, 930–942.
26 T. Sarma and P. K. Panda, *Chem. Rev.*, 2017, **117**, 2785–2838.
27 S. E. Braslavsky, M. Müller, D. O. Mártire, S. Pörting, S. G. Bertolotti, S. Chakravorti, G. Koç-Weier, B. Knipp and K. Schaffner, *J. Photochem. Photobiol., B*, 1997, **40**, 191–198.
28 A. G. Barrientos, J. M. de la Fuente, T. C. Rojas, A. Fernandez, S. Penades, A. Fernández and S. Penadés, *Chem. – Eur. J.*, 2003, **9**, 1909–1921.
29 M. J. Kamlet, J. L. M. Abboud, M. H. Abraham and R. W. Taft, *J. Org. Chem.*, 1983, **48**, 2877–2887.
30 C. Reichardt, *Solvents and Solvent Effects in Organic Chemistry*, Wiley-VCH Verlag GmbH & Co. KGaA, Weinheim, FRG, 2002.
31 J. Catalán, V. López and P. Pérez, *Liebigs Ann.*, 1995, **1995**, 793–795.
32 J. Catalán, V. López, P. Pérez, R. Martin-Villamil and J.-G. Rodríguez, *Liebigs Ann.*, 1995, **1995**, 241–252.
33 A. F. M. Barton, *Chem. Rev.*, 1975, **75**, 731–753.
34 M. J. Kamlet, P. W. Carr, R. W. Taft and M. H. Abraham, *J. Am. Chem. Soc.*, 1981, **103**, 6062–6066.
35 M. H. Abraham, R. M. Doherty, M. J. Kamlet, J. M. Harris and R. W. Taft, *J. Chem. Soc., Perkin Trans. 2*, 1987, 913–920.
36 H. A. Benesi and J. H. Hildebrand, *J. Am. Chem. Soc.*, 1949, **71**, 2703–2707.
37 R. C. Weast and M. J. Astle, *CRC Handbook of Chemistry and Physics*, CRC Press, Inc, Boca Raton, Florida, 60th edn, 1980, vol. 60.
38 J. Waluk, M. Muller, P. Swiderek, M. Kocher, E. Vogel, G. Hohlneicher and J. Michl, *J. Am. Chem. Soc.*, 1991, **113**, 5511–5527.
39 P. F. Aramendia, R. W. Redmond, S. E. Braslavsky, K. Schaffner, E. Vogel and S. Nonell, *Photochem. Photobiol.*, 1986, **44**, 555–559.
40 L. Forlani, P. De Maria and A. Fini, *J. Chem. Soc., Perkin Trans. 2*, 1980, 1156–1158.
41 L. Forlani and P. De Maria, *J. Chem. Soc., Perkin Trans. 2*, 1982, 535–537.
42 C. Öğretir, Ş. Demirayak and N. F. Tay, *J. Chem. Eng. Data*, 2006, **51**, 946–951.